



Study of Characterization Techniques of thin films

Dr. Shally Bhatia

Assistant Professor,
Department of Physics
Khalsa College for Women,
Amritsar 143001 (Punjab)

Abstract:

Tungsten oxide (WO_3) is a wide band gap semiconductor with unintentionally n-doping performance, excellent conductivity. Thin films of different thicknesses were deposited on fused silica, microscopy glass slide, single-crystal silicon wafer and alumina substrates and analyzed by Grazing Incidence X-ray Diffraction, UV-visible absorption and specular reflectance spectroscopy, AFM, FESEM and Raman spectroscopy. The interference fringes in the UV-visible transmittance and reflectance spectra are used to determine simultaneously, the thicknesses and refractive indices of amorphous and crystalline film samples. Several review on the characterization techniques of WO_3 has been published.

Keywords: Thin film, Characterization techniques, WO_3 , X-ray Diffraction, Raman spectroscopy

Introduction

Tungsten (VI) oxide, also known as tungsten trioxide or tungsten anhydride is an n-type semiconductor having chemical formula: WO_3 . It is a chemical compound containing oxygen and the transition metal, tungsten. It has indirect band gap which varies in a rather wide range: 2.5-3.5 eV. The amorphous WO_3 film have band gap of 3.1 eV while for crystalline film it is 2.9 eV [Berggren (2004); Ashan (2012)]. It has perovskite-like atomic configurations based on corner-sharing WO_6 octahedra, with the oxygen atom at the center of each octahedron [Johansson et al. (2013)]. The refractive index of the crystalline film varies in the range: 2.2–2.5 [Yaacob (2012); Berggren (2004)]. It has high melting point 1473 K. The oxidation state of W is 6+. The crystal structure of tungsten trioxide is dependent upon the temperature, the former changes with increase in temperature and gives



rise to several different phases like monoclinic, orthorhombic, tetragonal, triclinic etc., but the most stable phase is monoclinic which exists at room temperature. It exists in many different forms of oxides such as WO , WO_2 , WO_3 but the most stable oxide is WO_3 which is used in gas sensing and optical applications [Galatsis et al. (2002)]. It is obtained as an intermediate in the recovery of tungsten from its minerals. In this paper we have discussed the analytical techniques employed for the sample characterization. Thin film samples and nanoparticles were characterized by Grazing Incidence X-ray diffraction (GIXRD), UV-visible optical spectroscopy, electrical characterization, Field Emission Scanning Electron Microscopy (FESEM), Transmission Electron Microscopy (TEM), Atomic Force Microscopy (AFM) and Raman spectroscopy. Thin films and nanoparticles were studied for gas sensing applications towards H_2S and ethanol vapors.

Objective

The objective of this thesis is to study the structural, optical and gas sensing properties of tungsten trioxide and molybdenum trioxide thin films and nanoparticles and make structure-property correlations. Thin films of amorphous tungsten trioxide and amorphous molybdenum trioxide are grown by thermal evaporation and crystallized by post-deposition annealing in air. Thin films of different thicknesses were deposited on fused silica, microscopy glass slide, single-crystal silicon wafer and alumina substrates and analyzed by Grazing Incidence X-ray Diffraction, UV-visible absorption and specular reflectance spectroscopy, AFM, FESEM and Raman spectroscopy.

1. Grazing Incidence X-ray Diffraction (GIXRD)

X-ray powder diffraction is an analytical technique used for the study of size, structure, orientation and phase identification of a crystalline material and can provide information on unit cell dimensions. X-ray diffraction is based on constructive interference of monochromatic X-rays from a crystalline sample. It is a non-destructive technique. The X-rays are generated by a cathode ray tube, filtered to produce monochromatic radiation and directed towards the sample. The interaction of the incident rays with the sample produces

constructive interference (and a diffraction When condition satisfy Bragg's Law(this law relates the wavelength of electromagnetic radiation to the diffraction angle and the lattice spacing in a crystalline sample). X-ray photons are then detected, processed and counted.

Bragg's Law of diffraction is given by

$$2d\sin\theta = n\lambda \quad \dots(1)$$

Where d =interplanar spacing

θ = incident angle

λ =wavelength of incident X-ray n =

order of diffraction

Grazing Incidence X-ray Diffraction (GIXRD) is a scattering geometry combining the Bragg condition with the conditions for X-ray total external reflection from crystal surfaces as shown in **Fig.1**. Its superior characteristics as compared to the other diffraction techniques accomplish the structural characterization of thin films. The major application of GIXRD is to measure strain relaxation in thin layers and multilayers and it also measures lattice relaxation directly.

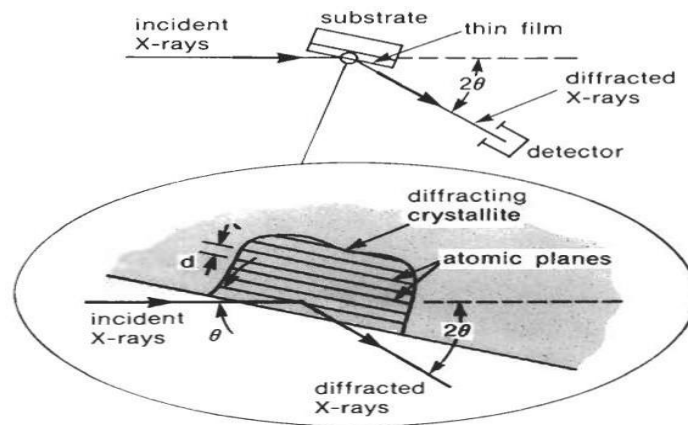


Fig.1:GIXRD geometry of XRD [Richard Brundle*et al.*(1992)].



$(\lambda = 1.54056 \text{ \AA})$ θ
GIXRD measurements were performed on thin film samples on Bruker D8 Focus X-ray diffractometer in the grazing incidence geometry with Cu-Kradiation. XRD studies were performed on thin film samples by keeping the incidence angle fixed at 2° and scanning the scintillation detector in the 2θ range of $10-70^\circ$. The tube was operated at 40kV and 35mA . The diffraction patterns were recorded with scanning speed of 1 s per step.

2. UV-Visible Spectroscopy

Ultraviolet–visible spectroscopy is basically an absorption or reflectance spectroscopy in the ultraviolet-visible region of the electromagnetic spectrum. It consists of the measurement of attenuation of a beam of light after passing it through a sample or after being reflected from a sample. It can be done at a single wavelength or over a wide spectral range. It is used to measure absorbance, reflectance and transmittance of the sample. Bandgap of the sample is determined from absorption measurements. The band gap of a semiconductor is of two types, a direct or an indirect band gap. The minimal-energy state in the conduction band and the maximal-energy state in the valence band are each characterized by certain crystal momentum (k -vector) in the Brillouin zone. If they are different, it is called an indirect gap. The band gap is called direct if the momentum of electrons and holes is the same in both the conduction band and the valence band; an electron can directly emit a photon. In an indirect gap, a photon cannot be emitted because the electron must pass through an intermediate state and transfer momentum to the crystal lattice.

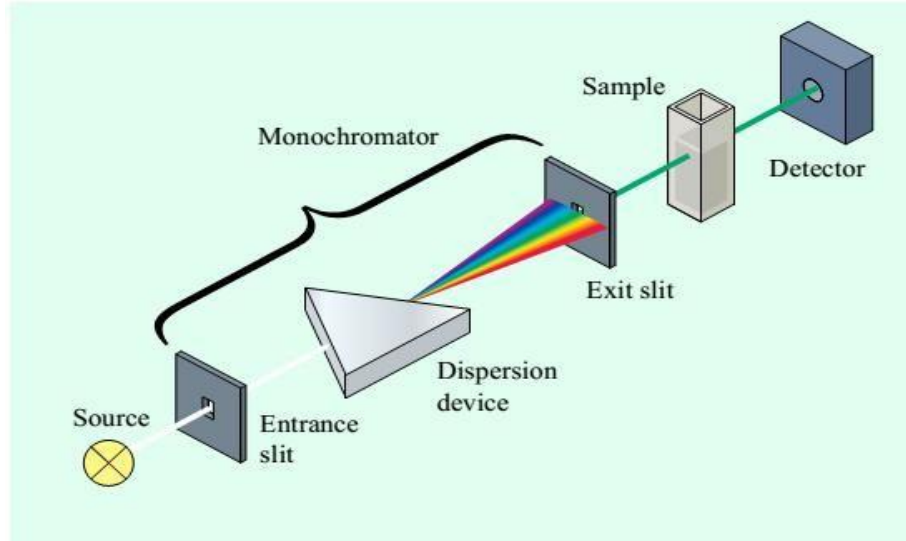


Fig.2: Basic diagram of instrumentation of UV-Visible spectrophotometer.

UV-visible specular reflectance and transmittance spectra were measured for both amorphous and crystalline films on Cecil UV-visible Reflect scan system in the wavelength range: 200-1100 nm. The thicknesses and the refractive index of films were calculated from the position of interference fringes in the reflectance and transmittance spectra.

The interference fringes in the reflectance and the transmittance spectra were used to determine simultaneously the refractive index, n and thickness, d of thin film amorphous and crystalline films. The formula of thickness using successive transmittance fringes is given by [Heavens (1965); Manificier *et al.*(1976)]:

$$d = \frac{\lambda_1 \lambda_2}{2(\lambda_1 - \lambda_2)n} \quad \dots(2)$$

where d is the film thickness, n is the refractive index, λ_1 and λ_2 are the wavelengths of two consecutive maxima. Similarly the formula of the thickness from fringes in the reflectance spectra is given by:

$$d = \frac{M}{2n^2} \left(\frac{\lambda_3 \lambda_4}{\lambda_3 - \lambda_4} \right) \quad \dots(3)$$

where d is the thickness, n is the refractive index, M is the number of fringes ($M=2$ for two successive fringes), λ_3 and λ_4 are the wavelength positions of two consecutive reflectance maxima.



By combining equations (3) and (4), the following formula was obtained and used for the measurement of refractive index:

$$n = \frac{(\lambda_1 - \lambda_2)M}{\lambda_1 \lambda_2} \left(\frac{\lambda_3 \lambda_4}{\lambda_3 - \lambda_4} \right) \quad \dots(4)$$

Having determined the refractive index, n from equation (4), the thickness, d of thin film sample was calculated by using equations (2) or (3).

Finally, the variation of refractive index, n with photon wavelength, λ was determined from the positions of two successive fringes in the reflectance spectra equation (4). The refractive index was fitted with Cauchy's dispersion formula [Heavens (1965)]:

$$n(\lambda) = A + \frac{B}{\lambda^2} \quad \dots(5)$$

The absorption coefficient, α was calculated from the transmittance and reflectance values by the relationship:

$$\alpha = \frac{1}{d} \ln \left(\frac{100-R}{T} \right) \quad \dots(6)$$

where d is the film thickness and R and T are % reflectance and transmittance values. WO_3 and MoO_3 are indirect band gap semiconductors and the band gap was calculated from the Tauc's relationship [Tauc (1968)]:

$$(\alpha h\nu)^n = A(h\nu - E_g) \quad \dots(7)$$

where A is a constant, $h\nu$ is the incident photon energy, E_g is the optical bandgap. For indirect transition the exponent takes the value $n=1/2$. The optical bandgap of WO_3 and MoO_3 thin films was determined by plotting graphs between $(\alpha h\nu)^{1/2}$ and photon energy ($h\nu$), and by extrapolating the straight line section of the plot to the energy axis.

3. Electrical Properties

The electrical conductivity of thin film samples was measured by two-probe set up by making two Al contacts on the top surface of thin films with a gap of about 1 cm between them. The variation of current with voltage was recorded at a regular interval of 2 V. The conductivity of films was calculated using the formula:



where R is the resistance of the film, w is width of the contacts, l is the length of gap between the contact and d is the thickness of the film. The conductivity increases exponentially with temperature and the relation between the conductivity and the temperature is given by:

$$\sigma = \sigma_0 \exp\left(-\frac{\Delta E_a}{kT}\right) \dots\dots\dots (9)$$

where σ is the conductivity at a temperature (T), σ_0 is a constant. From the Arrhenius plots the activation energy, ΔE_a of film is determined by:

$$\Delta E_a = 1000mk \dots\dots(10)$$

Where k is the Boltzmann constant and m is the slope of the linear fit curve.

4. Field Emission Scanning Electron Microscopy (FESEM)

The scanning electron microscope (SEM) utilizes a focused beam of high-energy electrons to generate a variety of signals at the surface of a sample. These accelerated electrons carry significant amounts of kinetic energy, and this energy is dissipated as a variety of signals produced by electron-sample interactions. These signals reveal information about the sample including external morphology (texture), chemical composition, crystalline structure and orientation of the sample [Zaefferer (2011)]. These signals include secondary electrons (that produce SEM images), backscattered electrons (BSE), diffracted backscattered electrons (EBSD) that are used to determine crystal structures and orientations. In most applications, data are collected over a selected area of the surface of the sample, and a 2-dimensional image is generated that displays spatial variations in these properties. The SEM is also capable of performing analyses of selected point locations on the sample.

Field Emission Scanning Electron Microscope (FESEM) has certain advantages over SEM because of its better resolution than SEM. The source of electrons in SEM is tungsten hairpin or LaB₆ while for FESEM the source is cold, thermal, or Schottky element. SEM does imaging up to micrometer resolution while FESEM can go up to few nanometer range. FESEM has more brightness and its filament has more lifetime in comparison to SEM. Therefore FESEM is better than SEM.

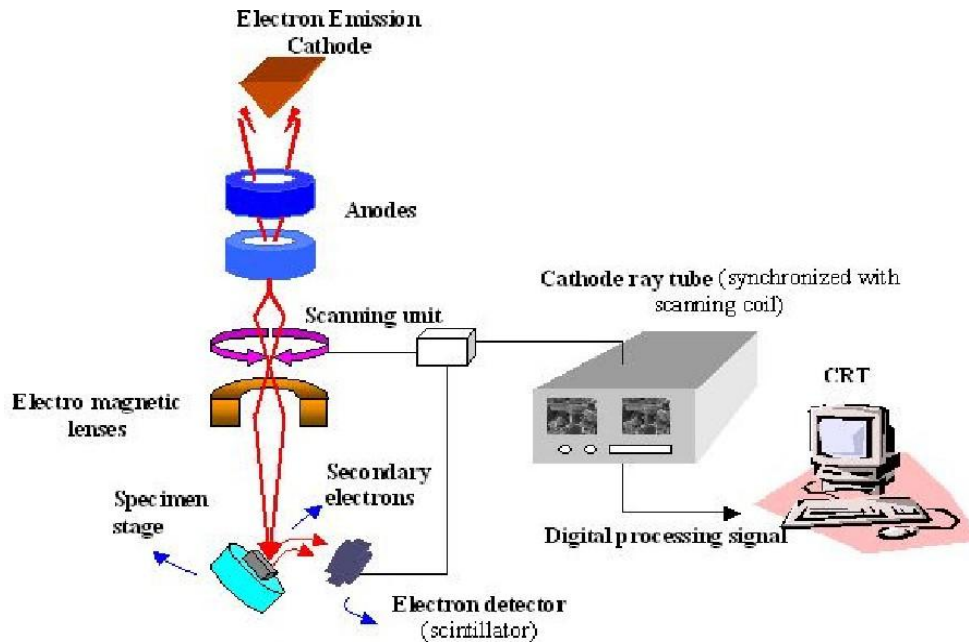


Fig.3:Systematic diagram of FESEM [Kumar (2011)].

The samples were coated with a thin gold layer prior to FESEM studies in order to reduce the surface charging effects. The elemental compositions of samples were measured by Energy Dispersive Spectroscopy (EDS) performed on X-Max 50 mm² detector (Oxford Instruments, UK).

Atomic Force Microscopy (AFM)

Atomic force microscope (AFM) is a very high-resolution type of scanning probe microscopy (SPM), with resolution of the order of fraction of a nanometer. Fig.3 illustrates the basic design and working principle of an AFM. It is used to measure the roughness of a surface at high resolution. AFM uses a cantilever with a very sharp tip to scan over a sample surface. As the tip approaches the surface, attractive force between the surface and the tip cause the cantilever to deflect towards the surface. However, as the cantilever is brought even closer to the surface, such that the tip makes contact with it, increasingly repulsive force takes over and causes the cantilever to deflect away from the surface [Binnig *et al.* (1986)].

AFM operation is usually described as one of three modes, according to the nature of the tip motion:

- contact mode, also called static mode
- tapping mode, also called intermittent contact
- non-contact mode

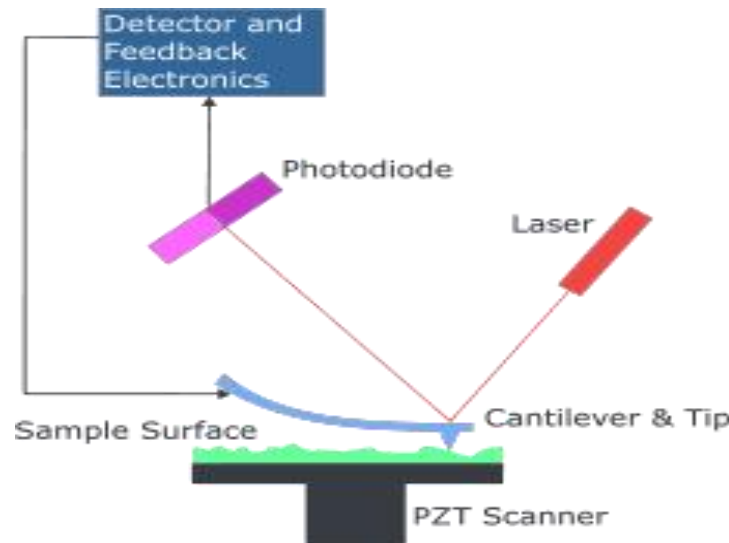


Fig.4: Systematic diagram illustrating the working principle of an AFM.

The cantilever provided with XE-70 was a silicon rectangular shaped cantilever for use in contact mode which had a small spring constant in the range: 0.01 to 3 N m^{-1} to respond with sensitivity to the tiny force between the atoms. The probe tip used in the contact mode had a thickness of about 1 m to achieve a small spring constant.

6. Transmission Electron Microscopy (TEM)

Transmission electron microscopy (TEM) is a technique in which a beam of high energy electrons is transmitted through an ultra-thin specimen, interacting with the specimen as it passes through. The basic schematic diagram of a TEM is given below (Fig.5). An image is formed from the interaction of the electrons transmitted through the specimen; the image is magnified and focused on to an imaging device, such as a fluorescent screen, photographic film, or a CCD camera. TEM is capable of

imaging at a significantly higher resolution than light microscopes, owing to the small de Broglie wavelength of electrons. This enables the instrument's user to examine the fine detail even as small as a single column of atoms, which is thousands of times smaller than the smallest resolvable object in a light microscope. At smaller magnifications TEM image contrast is due to absorption of electrons in the material, thickness and composition of the material. At higher magnifications complex electron-wave interactions modulate the intensity of the image.

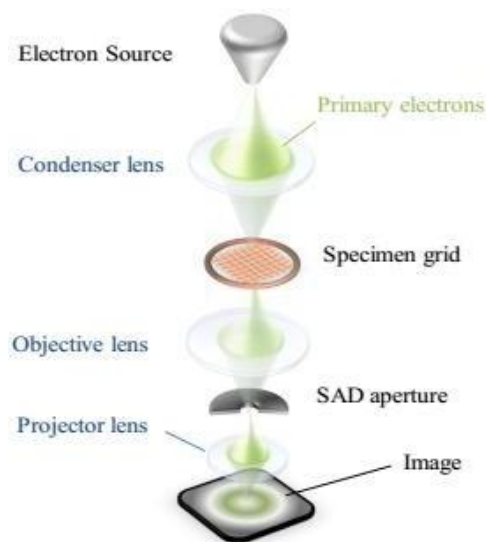


Fig.5: Systematic diagram of TEM [Yaacob(2012)].

The powdered sample was sprinkled on carbon coated copper grids and the d-spacing of interference fringes was determined. From d-spacing the crystal plane was identified.

7. Raman Spectroscopy

Raman spectroscopy is a technique which provides information about the vibrational, rotational and other low frequency transitions in molecules. It is based on inelastic scattering of monochromatic light, usually from a laser source in the visible, near infrared, or near ultraviolet range. Inelastic scattering means that the frequency of photons in monochromatic light changes upon interaction with a sample. Photons of the laser light are absorbed by the sample and then re-emitted. The laser light interacts with phonons or other

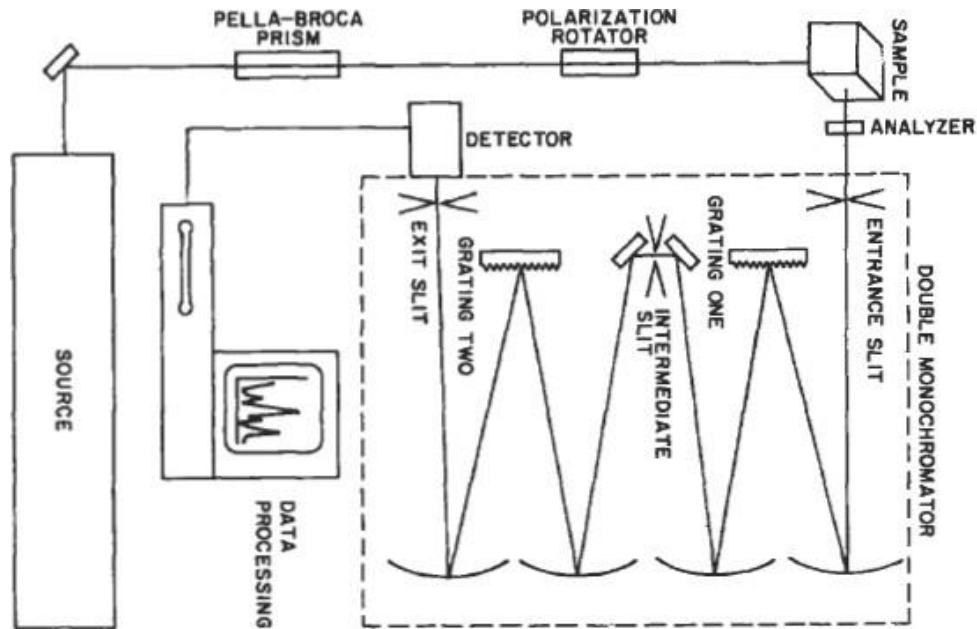


excitations in the system, resulting in the up or down shift of the energy of the laser photons. The shifting of the frequency (or wavenumber) of the scattered photons in comparison with original monochromatic frequency is called the Raman effect. The measurement of this shift by Raman spectroscopy can be used to study vibrational properties of solid and liquid samples.

$$P = \alpha E \quad \dots(11)$$

1. The intensity of the Raman scattering is seen to be proportional to the derivative of the polarizability(squared): thus, the polarizability must change linearly with vibrational motion for Raman scattering to occur A molecule with no Raman-active modes absorbs a photon with the frequency ν_0 . The excited molecule returns back to the same basic vibrational state and emits light with the same frequency ν_0 as an excitation source. This type of interaction is called an elastic Rayleigh scattering.
2. A photon with frequency ν_0 is absorbed by Raman-active molecule which at the time of interaction is in the ground vibrational state. The photon's energy is transferred to the Raman-active mode with frequency ν_m and the resulting frequency of scattered light is reduced to: $\nu_0 - \nu_m$. This Raman frequency is called Stokes frequency.
3. A photon with frequency ν_0 is absorbed by a Raman-active molecule, which at the time of interaction, is already in the excited vibrational state. Excessive energy of excited Raman active mode is released, the molecule returns to the basic vibrational state and the resulting frequency of scattered light goes up to $\nu_0 + \nu_m$. This Raman frequency is called Anti-Stokes frequency.

Fig.6.: The systematic diagram of a Raman spectrometer [Richard Brundle *et al.*



(1992)].

When a molecule is in an electric field E , the electron cloud and nuclei become polarized resulting in an induced dipole moment P . The size of the dipole moment induced by a field of magnitude E , classically is given by the polarizability, α of the molecule: The greater the change, the more intense is the Raman scattering. If α is unchanged or at a minimum/maximum, there is no Raman scattering. Since P and E are vector quantities. The polarizability tensor, α , is defined by nine coefficients (second rank tensor). However, because $\alpha_{xy} = \alpha_{yx}$, $\alpha_{zx} = \alpha_{xz}$, $\alpha_{yz} = \alpha_{zy}$ there are only six independent coefficients. Raman studies were performed on thin film and powdered samples of WO_3 and MoO_3 on Renishaw in Via Reflex micro Raman spectrometer equipped with a 514.5 nm and 488 nm Ar ion laser (50 mW), 2400 lines/mm diffraction grating, a suitable edge filter for recording the Stokes spectra and a CCD detector.

Conclusion

WO_3 and MoO_3 thin film samples were prepared by thermal evaporation on microscopy glass slide, fused-silica, silicon and alumina substrates. Characterization of coating samples was carried out by GIXRD, UV-visible absorption and reflection spectroscopy, electrical two-probe measurements, FESEM,



AFM and Raman spectroscopy. Thin film samples were annealed and the effects of post-deposition annealing on the structural, optical and electrical properties were studied.

References

Binnig, G., Quate, C. F. and Gerber, C. (1986). Atomic force microscopy. *Physical Review Letters* **56**: 930-933.

Heavens, O. S., Ed. (1965). *Optical Properties of Thin Solid Films*. Dover Publications, New York.

Kumar, S. (2011). *Methane, alcohol and carbon monoxide sensing of tin oxide-CNT nanocomposite sensors and molybdenum oxide sensors*. Master of Technology in Nanoscience & Technology, Thesis, Central Glass & Ceramics Research Institute (CGCRI), Kolkata, India.

Manifacier, J.C. Manifacier, J. C., Gasiot, J. and Fillard, J. P. (1976). A simple method for the determination of optical constants n , k and thickness of weakly absorbing thin film. *J. Phys. E* **9**: 1002.

Richard Brundle, C., Evans. Jr, C. A. and Wilson, S., Eds. (1992). *Encyclopedia of material characterization*. Manning Publications Co., Greenwich.

Tauc, J. (1968). Optical properties and electronic structure of amorphous Ge and Si. *Materials Research Bulletin* **3**: 37-46.

Yaacob, M.H. (2012). *Investigation of metal oxide nanostructured thin films based optical hydrogen sensors*. PhD Thesis, RMIT University, Australia.

Zaefferer, S. (2011). A critical review of orientation microscopy in SEM and TEM. *Crystal Research and Technology* **46**: 607-628.